RESONANCE AVOIDANCE OF VARIABLE SPEED ROTORS USING VARIABLE STIFFNESS BLADES

Mohammadreza Amoozgar, Faculty of Engineering, University of Nottingham, NG7 2RD, UK
Vilius Portapas, Faculty of Engineering, University of Nottingham, NG7 2RD, UK

Abstract

This paper presents and evaluates a new concept for resonance avoidance of variable speed rotors. This concept is based on using a Variable Stiffness (VS) composite spar, which mechanical properties can be varied in flight. This adaptive spar is made of a mixture of composite laminates and variable stiffness layers. The variable stiffness layers are made of shape memory alloy fibers and their module of elasticity can be changed or controlled by the addition of heat. To model the structural dynamics of the blade, a one dimensional geometrically exact beam formulation has been coupled with a two dimensional cross-sectional analysis tool. The rotating frequencies of the blade are obtained by finding the eigenvalues of the linearized equations about the nonlinear steady-state condition. First the accuracy of the developed model is verified against available results for a scaled composite blade, and a very good agreement is observed. Next, the effect of adding variable stiffness layers on the blade frequencies is examined. It is found that by changing the temperature of the blade by only 10 degrees, it is possible to modify the resonance frequencies. This is obtained by either removing the resonance crossing from the operational range or moving the crossing toward higher harmonics. Finally, the proposed concept is applied to a full-scale blade and the same observations are obtained.

1. NOTATION

Symbols

$\mathbf{A}$, $\mathbf{B}$, $\mathbf{C}$	Components of flexibility matrix
$\mathbf{F}$, $\mathbf{M}$	Internal force and moment
h	Spar height
$\mathbf{I}$	Mass moment of inertia
L	Rotor radius
$\mathbf{P}$, $\mathbf{H}$	Linear and angular momentum
t	Spar wall thickness
$\mathbf{V}$, $\mathbf{\Omega}$	Linear and angular velocities
w	Spar width
β	Extention-twist coupling
Ω_{ref}	Rotor speed of rotation
μ	Mass per unit length
$\boldsymbol{\gamma}$ and $\boldsymbol{\kappa}$	Strain and curvature measures
$\boldsymbol{\xi}$	Centre of mass offset from reference axis

2. INTRODUCTION

It is anticipated that the future global aerospace market will move toward greener products to cut emissions. This is because one of the main challenges that the world is facing now is climate change. Therefore, almost all international governments agreed to reduce their carbon footprint so that the global warming be well below 2^{o}C. The global aviation industry, alone, produces about 3% of global carbon emissions and high levels of NOx emissions. Therefore, to achieve the net-zero 2050 target, novel and breakthrough solutions/technologies, such as hybrid aircraft, more efficient aircraft, hydrogen-based engines, etc., are required. The Advisory Council for Aeronautics Research in Europe has set a goal to reduce the CO_2 and NOx emissions by 50% to 80% for new aircraft [1]. One of the promising concepts toward more efficient rotorcraft is the concept of variable speed rotor (VSR), and Prouty presented the benefits that a VSR could provide [2]. This concept has received an increasing interest over the past two decades [3-5]. It has been identified that the Figure of Merit of the rotor in hovering condition happens at different rotational speed for different altitudes [6]. Also, Steiner [7] showed that the main rotor power of the UH-60 Black Hawk helicopter can be reduced by 15% by varying the rotor speed. Mistry and Gandhi [8] investigated the effects of varying rotor speed combined by varying rotor radius on the performance improvement of the rotorcraft. VSR concept has already been implemented in several products such as V-22 Osprey, AW-609, Bell 407, XH-59, and others [2]. Also, recently this concept has attracted attention of the advanced air mobility community due to their improved efficiency (e.g. Jaunt Air Mobility and Overair's Butterfly). The concept of variable speed rotor contrasts with conventional helicopters where usually the main rotor rotates at a constant speed. There are several reasons that a rotorcraft operates at a constant speed, but one of the main issues is the vibration of the rotor due to passing through resonance points during speed change [5].

There are three potential ways to overcome this challenge. The first solution could be to design a rotor system which is able to sufficiently separate the natural and excitation frequencies for a wide range of rotating speeds. This is very challenging as the blade design itself is always a compromise between several conditions, and hence not always a feasible option. The second option can be to reduce the blade vibratory loads (rather than removing the resonance conditions) using passive (e.g. embedded dampers) or active (e.g. trailing edge flaps) vibration control methods. Although active and passive vibration control methods are workable solutions, they also have their own challenges [3]. Alternative to these two options, there is a third option which is to avoid the resonance conditions in flight which potentially have some benefits over the previous methods [3]. It is noted that designing a very stiff blade which natural frequencies are higher than the excitation frequencies for resonance avoidance is not a viable option as this can increase the blade mass by up to 34% [9]. Dibble et al. [3] introduced a new concept for resonance avoidance for VSRs. In this method, a compressive force is applied to the blade to separate the blade natural frequencies and excitation frequencies in flight. They showed that it is possible to reduce the blade natural frequencies by up to 10% to avoid the resonance situations in different conditions. Chandrasekaran and Hodges [2] showed that the lag stiffness of the blade has a direct impact on the natural frequencies of the blade, and hence properly designing the lag stiffness can result in resonance avoidance. However, they showed that a blade with high lag stiffness can introduce other challenges such as higher torque responses. More recently, an adjustable tendon supported by dynamically tuned squeeze film damper guides concept has been proposed to suppress the blade resonance vibration [10]. It has been shown that this concept is able to introduce highly focused blade damping to reduce the vibration amplitude.

In the last few years, a new interest has arisen toward the application of the concept of variable stiffness structures. Ondra et al. [11] proposed an active vibration suppression for truss structures using variable stiffness members. The axial stiffness of the member was varied by a small stroke of piezoelectric actuators, and the results indicated that this concept can be effective for realistic structures. Gandhi and Kang [12] developed another concept to vary the flexural bending stiffness of a multi-layer beam. This has been done by adding polymer layers on top and bottom surfaces of the beam. The experimental results showed that the flexural stiffness of the beam can be varied by up to four times when the temperature increases. A variable stiffness spar has been proposed by Chen et al. [13] to improve the roll performance of the aircraft. The stiffness change of the wing was obtained by rotating the spar by suing actuators, and it was shown that it is possible to improve the roll performance by up to 22%. Raither et al. [14] studied the efficiency and performance of using a variable stiffness element for morphing of a plate. The variable stiffness plate was able to produce an adaptive bending-twist coupling by adding polymer layers to the laminates. The results of this study showed that the bending-twist coupling of the plate can be varied by up to 10 times by changing the plate temperature.

The contribution of this paper is to investigate the effectiveness of using a variable stiffness spar (VSS) for resonance avoidance and load reduction of variable speed rotors. The spar is made from a mixture of composite and variable stiffness (VS) layers, and the effects of increasing the temperature and number of VS layers on the rotating frequencies of the blade are determined.

3. Problem Statement

A composite hingeless rotor blade with variable stiffness spar, as shown in Figure 1, is considered. The main structure of the blade is assumed to be a rectangular closed section spar. The spar is made from several layers of composite laminates and VSS layers as shown in Figure 1. The blade length is denoted by L and it rotates with a rotational speed of Ω_{ref} around the z axis. Furthermore, the spar width, height and wall thickness are denoted by w, h, and t, respectively. It is noted that in this study, only an anti-symmetric layup is considered where the extension-twist coupling is dominant in the cross-sectional stiffness matrix as will be discussed later.

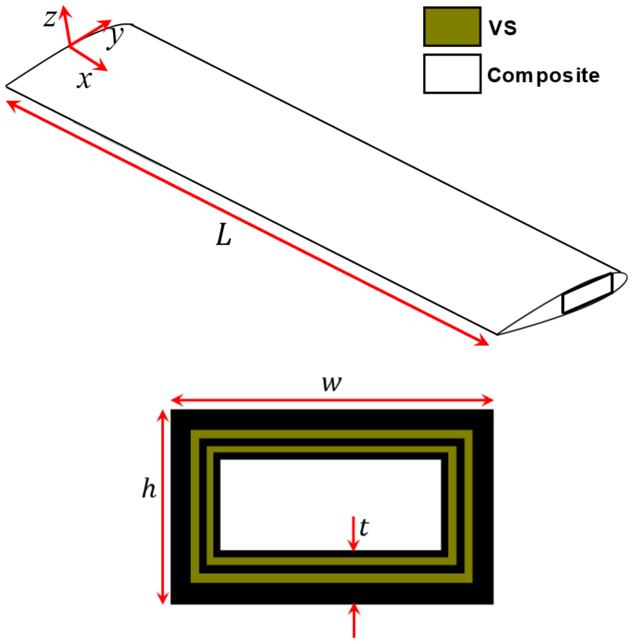

Figure 1: The schematic of the blade with variable stiffness spar

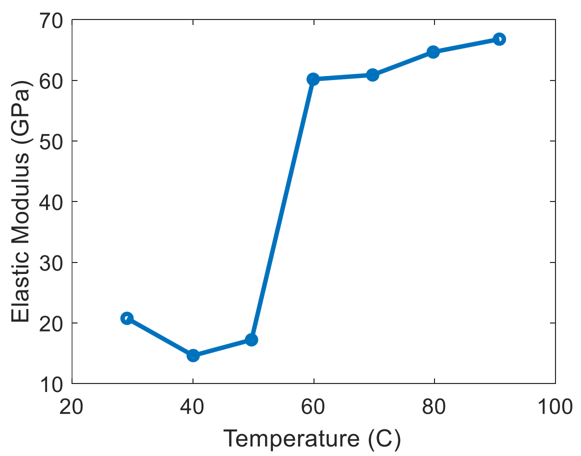

Figure 2: The elastic modulus of Nitinol vs temperature [15]

It is assumed that the variable stiffness layers are made from shape memory alloy (SMA) hybrid composites that contain shape memory alloy fibers in such a way that the module of elasticity of these layers can be changed or controlled by the addition of heat [16]. Here it is assumed that the SMA fibers are made from Nitinol. Nitinol is a nickel-titanium alloy that exhibits shape memory effect. Above the austenite temperature, its stiffness increases and below martensite its stiffness decreases. Figure 2 shows the Young's modulus of nitinol versus temperature [15]. A jump in elastic modulus is seen at the transition from martensite to austenite between 50º and 60º.

Mathematical Modelling

The structural dynamics of the blade is simulated by combining a 1D beam model with a 2D cross-sectional analysis. To model the 1D global behavior of the beam, the geometrically exact fully intrinsic beam equations are used [17]

$$\begin{gathered} \mathbf{F}' + (\tilde{\mathbf{k}} + \tilde{\boldsymbol{\kappa}})\mathbf{F} = \dot{\mathbf{P}} + \tilde{\boldsymbol{\Omega}}\mathbf{P} \\ \mathbf{M}' + (\tilde{\mathbf{k}} + \tilde{\boldsymbol{\kappa}})\mathbf{M} + (\tilde{\mathbf{e}}_1 + \tilde{\boldsymbol{\kappa}})\mathbf{F} = \dot{\mathbf{H}} + \tilde{\boldsymbol{\Omega}}\mathbf{H} + \tilde{\mathbf{V}}\mathbf{P} \\ \mathbf{V}' + (\tilde{\mathbf{k}} + \tilde{\boldsymbol{\kappa}})\mathbf{V} + (\tilde{\mathbf{e}}_1 + \tilde{\boldsymbol{\gamma}})\boldsymbol{\Omega} = \dot{\boldsymbol{\gamma}} \\ \boldsymbol{\Omega}' + (\tilde{\mathbf{k}} + \tilde{\boldsymbol{\kappa}})\boldsymbol{\Omega} = \dot{\boldsymbol{\kappa}} \end{gathered} \tag{1}$$

where $\mathbf{F}$, $\mathbf{M}$, $\mathbf{V}$ and $\boldsymbol{\Omega}$ are vectors of the internal force, internal moment, generalized linear velocity and generalized angular velocity, respectively. Also, $\boldsymbol{\gamma}$ and $\boldsymbol{\kappa}$ are the generalized strain and curvature, which are obtained using the internal force and moment

$$\begin{bmatrix} \boldsymbol{\gamma} \\ \boldsymbol{\kappa} \end{bmatrix} = \begin{bmatrix} \mathbf{A} & \mathbf{B} \\ \mathbf{B}^T & \mathbf{C} \end{bmatrix} \begin{bmatrix} \mathbf{F} \\ \mathbf{M} \end{bmatrix} \tag{2}$$

where $\mathbf{A}$, $\mathbf{B}$, and $\mathbf{C}$ are the beam cross-sectional flexibilities. Moreover, $\mathbf{P}$ and $\mathbf{H}$ are vectors of generalized linear and angular momentum which are obtained using the generalized velocities and cross-sectional mass matrix as follows

$$\begin{bmatrix} \mathbf{P} \\ \mathbf{H} \end{bmatrix} = \begin{bmatrix} \mu\boldsymbol{\Delta} & -\mu\tilde{\boldsymbol{\xi}} \\ \mu\tilde{\boldsymbol{\xi}} & \mathbf{I} \end{bmatrix} \begin{bmatrix} \mathbf{V} \\ \boldsymbol{\Omega} \end{bmatrix} \tag{3}$$

where μ is the beam mass per unit length, $\boldsymbol{\Delta}$ is the identity matrix, and $\mathbf{I}$ and $\boldsymbol{\xi}$ are the mass moment of inertia matrix, and offsets of the cross-section mass centre from the beam reference axis, respectively. By substituting the above equations into the main governing equations, the final nonlinear structural dynamics equations of the blade are obtained. To solve the resulting equations, a second-order accurate discretization method as explained in [17] is used. The rotating frequencies of the blade are obtained by finding the eigenvalues of the linearized equations about the nonlinear steady-state condition [18, 19].

4. Results and Discussions

In this section, the developed numerical model is first validated against published results. Then, parametric studies are carried out to evaluate the effectiveness of the proposed concept for resonance avoidance of variable speed rotor blades.

In order to verify the developed method, a composite hingeless rotor blade with a rectangular composite cross-section as described in [20] is considered first. Each wall of the composite box is made of 6 layers, and they are arranged in a symmetric way to produce a bend-twist coupling. The comparison between the rotating frequencies is presented in Table 1, and a very good agreement is observed. It is noted that 16 elements have been used to discretize the blade.

Table 1: Comparison of the rotating frequencies of the composite beam with symmetric layup of $[15]_6$, $[15/-15]_3$ at $\Omega = 1002$ rpm.

Mode	Present	Detailed FEM [20]
Flap 1	35.741	36
Lag 1	56.854	57.1
Flap 2	197.01	197.3
Lag 2	350.26	349.3
Torsion 1	713.92	714.9

A composite scaled helicopter blade is considered as a baseline configuration [21]. The blade spar is made of AS4/3501-6 graphite/epoxy, and the spar box outer width and height dimensions are *w*=12.804 mm and *h*=8.944 mm. The rectangular box-spar has four walls, and each wall consists of 6 layers with a total thickness of *t*=0.804 mm. The blade properties are listed in Table 2 and its material properties are summarized in Table 3.

Table 2: The hingeless rotor blade properties.

Parameter	Value
Blade length (L)	0.9615 m
Mass per unit length (μ)	0.343 (kg/m)
Polar mass moment of inertia (i_{11})	2.062×10^{-4} (kg.m)
Rotor baseline speed (Ω_{ref})	1000 (rpm)

Table 3: The material properties of AS4-3501-6.

Parameter	Value
E_{11} (GPa)	142
$E_{22} = E_{33}$ (GPa)	9.8
$G_{12} = G_{13}$ (GPa)	6.0
G_{23} (GPa)	3.77
$\upsilon_{12} = \upsilon_{13}$	0.3
υ_{23}	0.34
ρ (kg/m^3)	1445

Here, only one layup case with ξ ply angle is considered where the extension-twist (E-T) coupling is dominant as presented in Table 4. It is noted that in future studies other types of couplings will be considered as well.

Table 4: The blade layup cases.

Case	Top	Bottom	Left	Right
(E-T)	$[\xi]_6$	$[-\xi]_6$	$[\xi]_6$	$[-\xi]_6$

In the first step, to understand the effect of different ply angles on the dynamics of the blade, the rotating frequencies of the baseline blade with this layup is determined and shown in Figure 3.

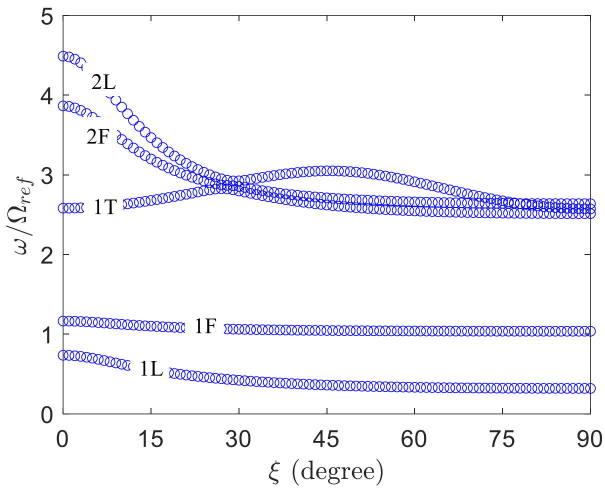

Figure 3: The rotating frequencies of the baseline blade

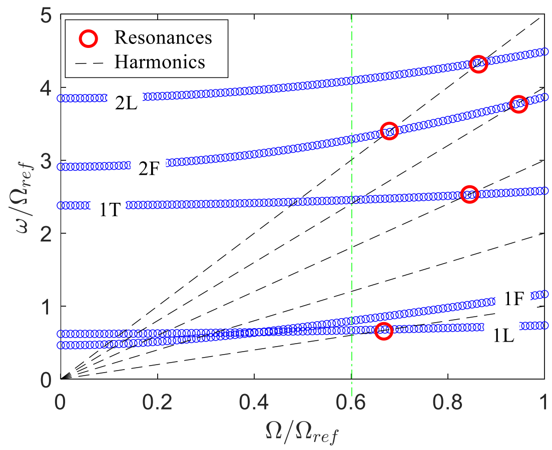

Figure 4: The Campbell diagram for the blade with ply angle $\xi = 0^o$

As it has been mentioned before, here it is assumed that the rotating speed of the rotor can be varied to improve its performance [5]. Here the transition speed is considered between 60% to 100% of the rotor speed as also considered in [3]. Figure 4 shows the

Campbell diagram of the rotor for $\xi = 0^o$. It is clear that when the blade is rotating in nominal condition (e.g. $\Omega/\Omega_{ref} = 1$), no resonance point is available. However, if the rotor needs to be running in the transition speed range ($0.6 \leq \Omega/\Omega_{ref} \leq 1$), there are several resonance points that the rotor faces which could lead to high vibratory loads, and hence, it would be beneficial to find a way to remove these crossing points from the operational speed range.

To do this, it is assumed that some layers of the composite spar are replaced with variable stiffness SMAs. First, it is assumed that only the second and fourth layers of the spar are made from hybrid composite as discussed above. The effect of temperature on the flap, lag and torsional stiffness changes of the box is determined and shown in Figure 5 with respect to the baseline values. It is clear that the stiffness of the blade now is variable and depends on the temperature of the variable stiffness layer. It is noted that the highest change is seen in the torsional stiffness by up to 70% when the temperature changes from 50º to 60º, while the flap and lag stiffness values change only by about 10%.

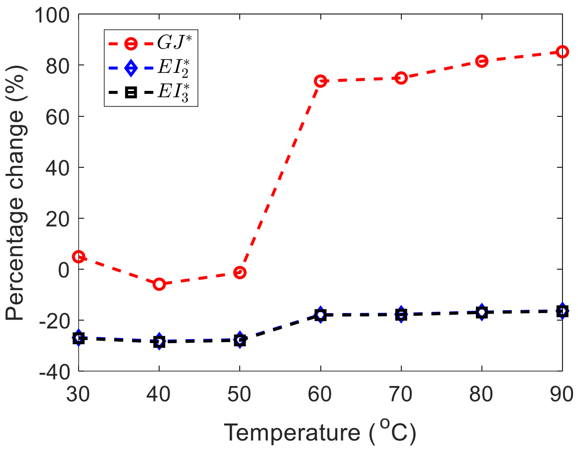

Figure 5: The change in cross-sectional stiffness of the blade versus temperature for ply angle $\xi = 0^o$

Figure 6 shows the nondimensional extension-twist coupling of the blade versus ply angle for the blade with and without variable stiffness layers and for different temperatures. It is noted that here the nondimensional extension-twist coupling is obtained as follows

$$\beta = \frac{S_{14}}{\sqrt{S_{11} \times S_{44}}}$$

where, S_{11}, S_{44} and S_{14} are the axial, torsional and extension-twist coupling stiffnesses, respectively. It is obvious that the elastic coupling of the blade can also be altered as the temperature increases. In what follows, a parametric study is done to understand the impact of variable stiffness layers on the rotating frequencies of variable speed rotors.

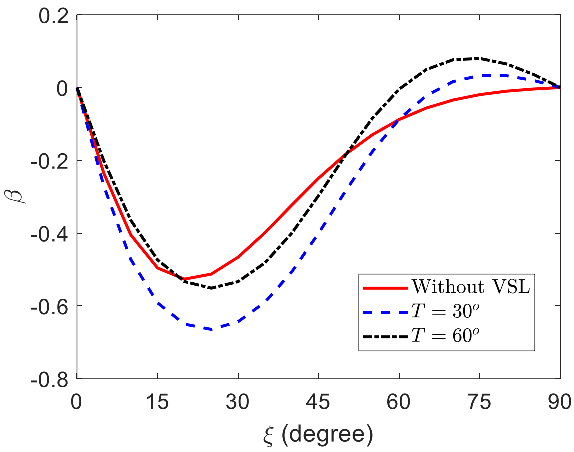

Figure 6: The change in nondimensional extension-twist coupling for various temperatures and ply angles

Table 5 and

Table *6* show the effect of temperature on the first five natural frequencies of the blade with $\xi = 0^o$ at $\Omega/\Omega_{ref} = 0$ and $\Omega/\Omega_{ref} = 1$, respectively. Here, the percentage difference of the frequencies are calculated with respect to the baseline blade. As expected, the highest change happens when the temperature increases to 60º.

Table 5: The blade frequencies at $\Omega/\Omega_{ref} = 0$.

Temp	1F (%)	1L (%)	1T (%)	2F (%)	2L (%)
30º	-14.42	-14.64	2.39	-14.10	-14.27
40º	-15.26	-15.49	-3.02	-15.02	-15.20
50º	-14.91	-15.13	-0.69	-14.63	-14.80
60º	-9.26	-9.43	11.70	7.79	-8.75
70º	-9.17	-9.34	11.81	8.17	-8.66
80º	-8.70	-8.86	12.42	10.19	-8.16
90º	-8.43	-8.59	12.76	11.31	-7.88

Table 6: The blade frequencies at $\Omega/\Omega_{ref} = 1$.

Temp	1F (%)	1L (%)	1T (%)	2F (%)	2L (%)
30º	-10.76	-2.43	2.06	-7.66	-10.21
40º	-11.43	-2.59	-2.54	-8.16	-10.87
50º	-11.14	-2.52	-0.57	-7.95	-10.59
60º	-6.77	-1.50	27.56	-4.68	-6.26
70º	-6.70	-1.49	27.97	-4.63	-6.20
80º	-6.34	-1.40	30.14	-4.36	-5.84

90º	-6.13	-1.35	31.34	-4.21	-5.64

Next, the effect of temperature variation on the resonance avoidance of the blade is considered and the results are presented in Figure 7 for ply angle of $\xi = 0^o$. It is obvious that as the temperature increases, the resonance points are shifting which could be a way of resonance avoidance. In this case, the highest shift in frequency is seen for torsional mode, and the lowest shift is evidence for first lag and flap modes.

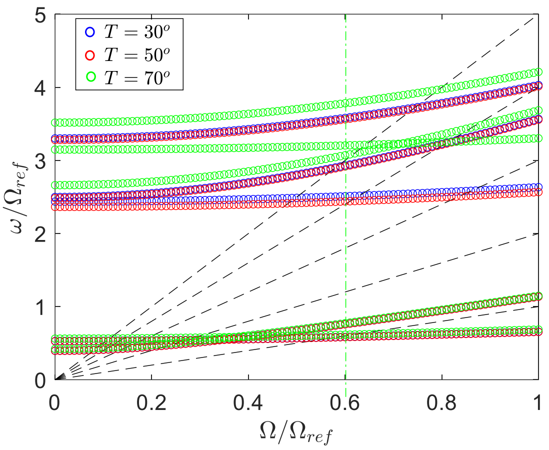

Figure 7: The effect of temperature variation on the rotating frequencies of the blade for ply angle $\xi = 0^o$

To have a closer look at the separation between rotating and excitation frequencies, a nondimensional variable, Modal Separation (MS), is defined here. It is noted that an increase in the MS value means the separation between excitation and rotating frequencies increases, and MS=0 refers to a resonance point at a specific rotating speed.

$$\text{MS} = \frac{\min\left(|\omega(\Omega) - n\Omega|\right)}{\Omega}$$

So, the calculated minimum modal separation (MMS) of the diagram shown in Figure 7 is present in Figure 8 for each mode and up to 5/rev harmonics. It is noted that the minimum acceptable level of separation has been mentioned in the literature as to be 10% of the rotor speed, and hence this line has been drawn alongside the MSS values. It is clear that by increasing the temperature, the first flap and lag modes are slightly affected, but the location at which the resonance occurs has shifted. It must be noted that when the temperature increases, an extra resonance point occurs for first lag mode at around $\Omega/\Omega_{ref} = 0.62$. Also, it is obvious that the temperature works better for flap mode compared to the lag mode. Furthermore, the temperature is helpful for second lag mode compared to second lag mode, as it increases the MSS value for all rotating speeds. Although the MSS of the first torsion mode doesn't show too much benefits, but as it is clear from Figure 8, the resonance point of this mode is shifted toward higher harmonics (e.g. from 3,4/rev to 4,5/rev). This has the benefit of reducing the resonance loads, as when the crossings happen at higher harmonics, the blade response/load will be less severe than when the crossing happens at lower harmonics [2].

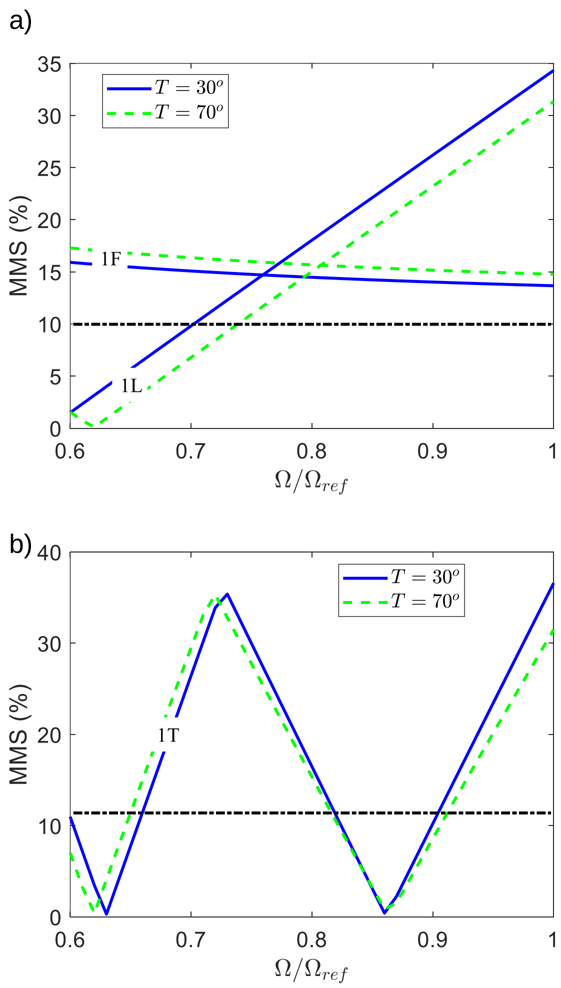

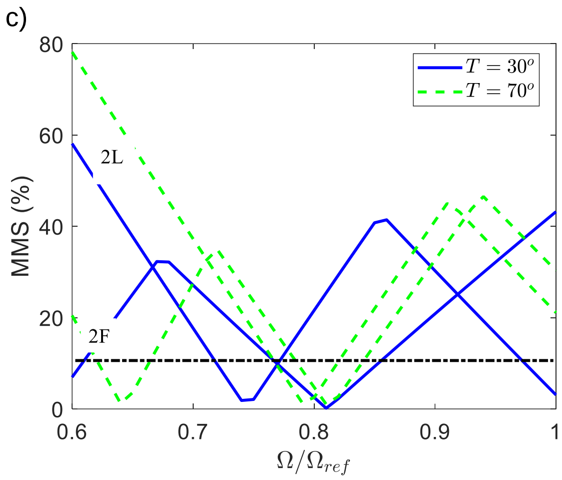

Figure 8: The effect of temperature on the MSS value for ply angle $\xi = 0^o$, and for a) first flap and first lag, b) first torsion, c) second flap and lag modes

Next, the effect of elastic coupling combined with temperature on the rotating frequencies of the blade is investigated. Figure 9 shows the Campbell diagram and resonance crossings of the composite blade without VSL and for ply angle $\xi = 15^o$. As it is clear, in this case the resonance only happens for first torsion and second flap and lag modes.

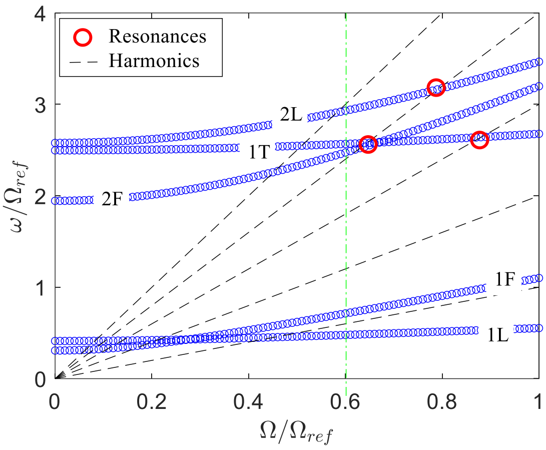

Figure 9: The Campbell diagram for case 3 with ply angle $\xi = 15^o$

The effect of temperature on the resonance avoidance of this case ($\xi = 15^o$) is considered and the results are presented in Figure 10 and Figure 11. Again temperature change can result in change at the location at which the resonance happens.

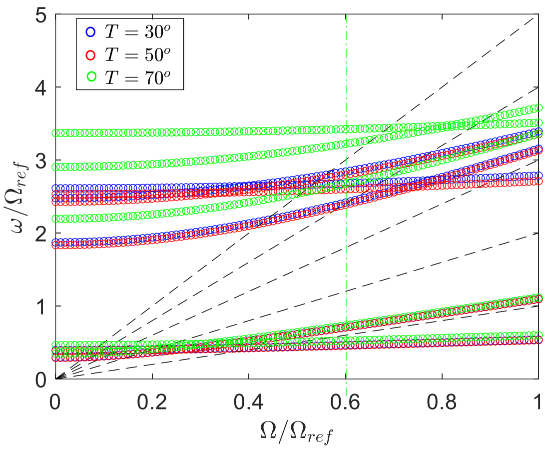

Figure 10: The effect of temperature variation on the rotating frequencies of the blade for ply angle $\xi = 15^o$

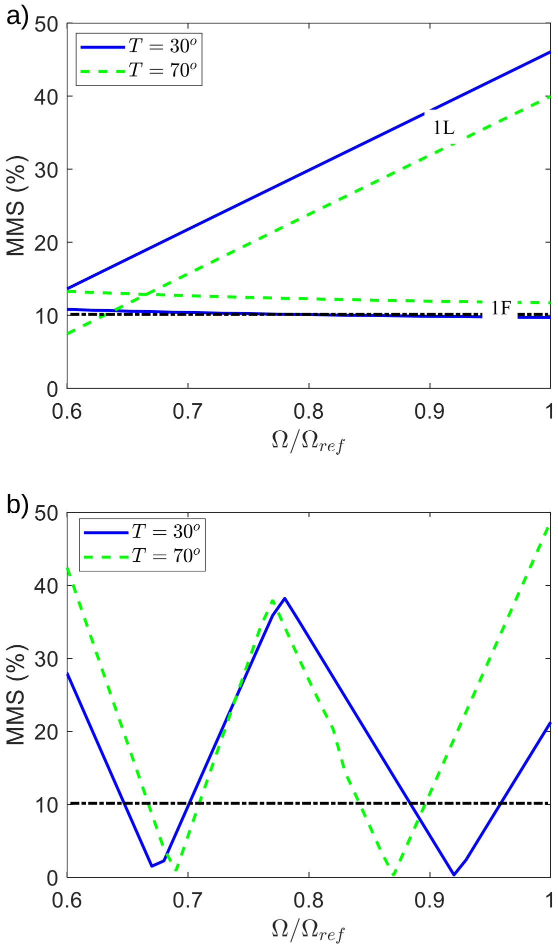

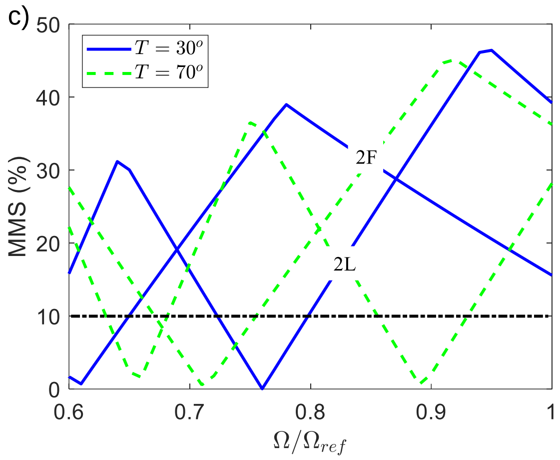

Figure 11: The effect of temperature on the MSS value for ply angle $\xi = 15^o$, and for a) first flap and first lag, b) first torsion, c) second flap and lag modes

By now, it has been showed that using VSLs would influence the resonance behavior of the blade. But, the effect of the number of VSLs has not been considered. Hence, Figure 12 and Figure 13 summarizes the resonance points for various modes and number of layers of VSLs for two ply angles. As the number of VS layers changes, the resonance points also change, but the behavior is different among different modes. For instance, as shown in Figure 12 (a), when the number of layers increases to 3, the resonance is completely removed from the operational range of the rotor. Also, the number of layers can change the number of resonance crossings for each individual modes, as shown in Figure 12 (c).

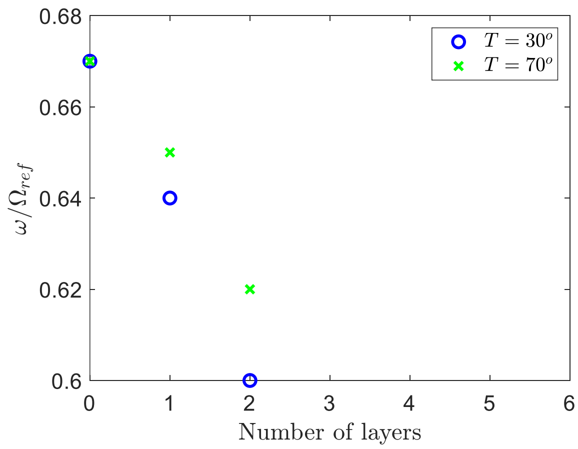

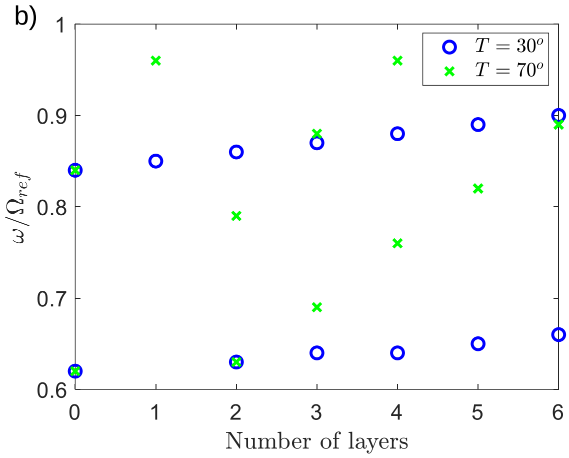

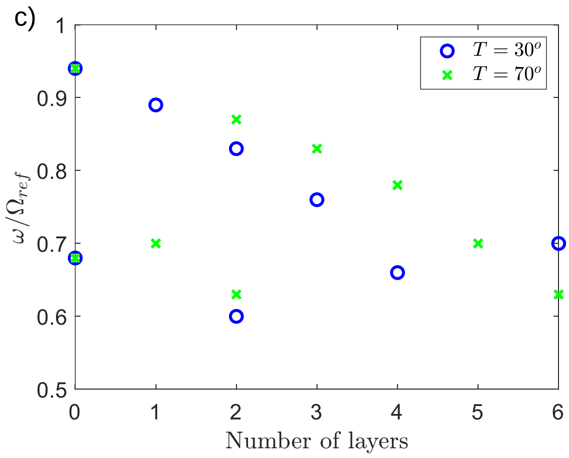

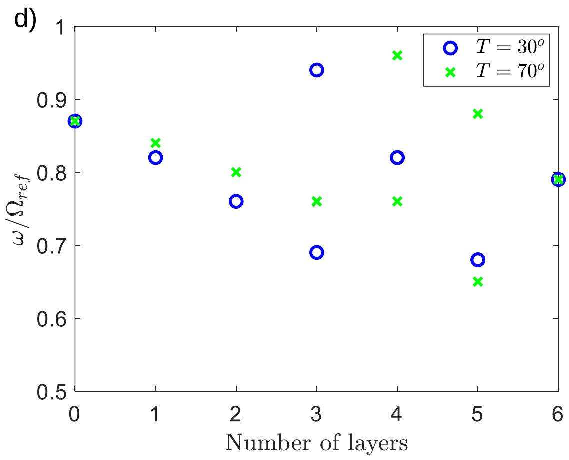

Figure 12: The effect of number of layers on the first resonance points for ply angle $\xi = 0^o$, and for a) first lag, b) first torsion, c) second flap and d) second lag modes

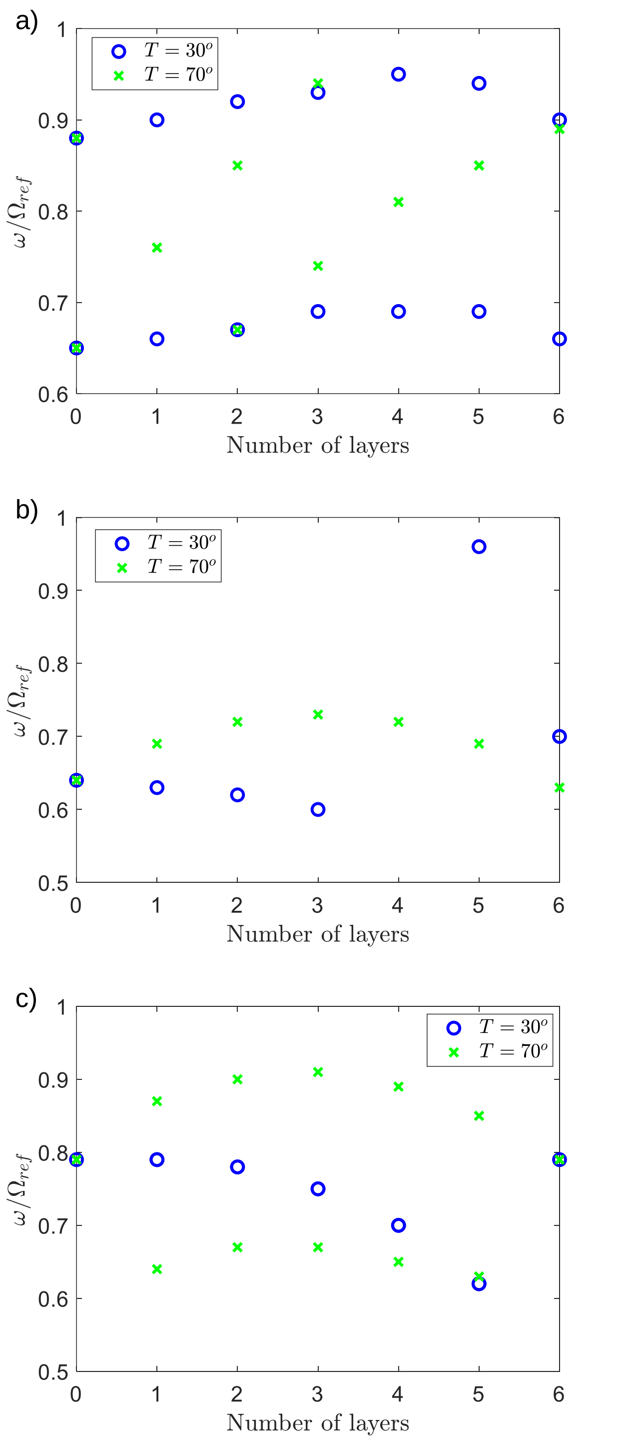

Figure 13: The effect of number of layers on the first resonance points for ply angle $\xi = 15^o$, and for a) first torsion, b) second flap and c) second lag modes

Finally, to evaluate of the proposed concept on more realistic blade, a full scale blade with the properties presented in [2] is considered. Based on the stiffness change that variable stiffness layers can provide for a blade, as shown in Figure 5, it is assumed that the flap, lag and torsional stiffness values can be altered by 20% when the temperature changes from 30º to 60º which has been shown to be feasible. Figure 14 shows the Campbell diagram of this full scale blade alongside the resonance crossing points that happens in the operational speed range ($0.8 \leq \Omega/\Omega_{ref} \leq 1$) .

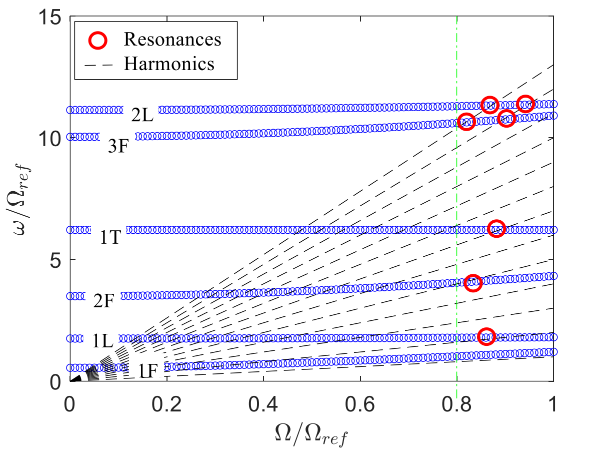

Figure 14: The Campbell diagram of the full scale blade

There are several resonance points that are happening in the operational range of the rotor speed. Here, the focus would only be on the first three crossing points (e.g. first lag, second flap and first torsion). Figure 15 shows the variation of these crossing points of these three modes for changes of lag, flap and torsional stiffness values due to temperature.

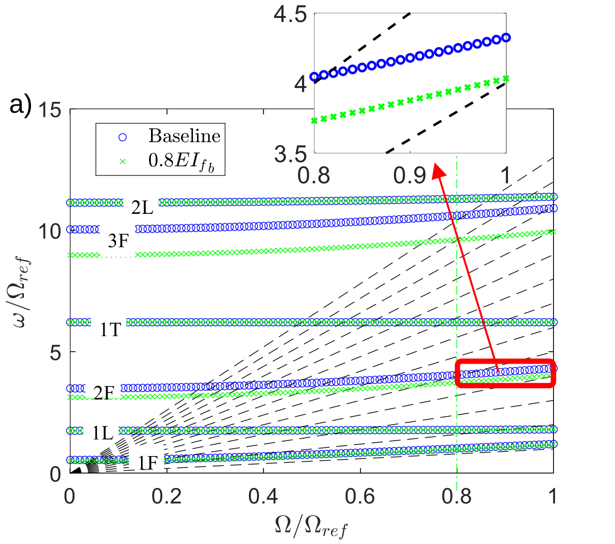

b)

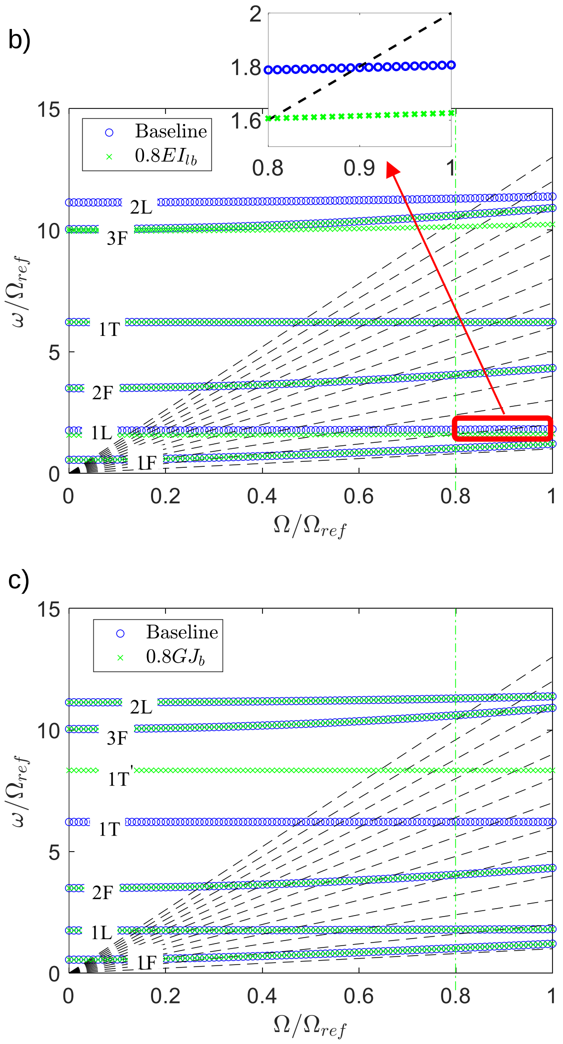

Figure 15: The change in blade resonance points with the change in a) flap stiffness, b) lag stiffness and c) torsional stiffness

When the flap stiffness decreases by 20%, the resonance that happened initially at $\Omega/\Omega_{ref} = 0.81$ has not been removed from the speed range. Same observation is seen for the lag mode crossing. For the torsional mode, when the torsional stiffness decreases, the resonance points shift toward higher harmonics (e.g. 7/rev,8/rev to 9/rev and 10/rev). This clearly shows that using a variable stiffness mechanism, it is possible to shift or remove the resonance points from the operational range of speeds of the rotor. However, it is still necessary to understand how this can impact the vibratory loads of the blade. This will be investigated in future studies.

5. CONCLUSIONS

In this paper, the effectiveness of a variable stiffness spar on resonance avoidance of a variable speed rotor was investigated. The blade spar was made from composite laminates combined by shape memory alloy hybrid composites of which their material properties can be varied by increasing the temperature. The blade dynamics was simulated using an exact beam theory, and the blade frequencies are obtained by obtaining the eigenvalues of the linearized equation of motion about the steady-sate condition. An anti-symmetric laminate layup was considered where an extension-twist coupling is available, and the effect of temperature on the rotating frequencies of the blade were determined. It was found that when the blade temperature increases by only 10^{o}, the flap, lag and torsional stiffnesses of the blade can be changed. This is the main mechanism of varying the rotating frequencies of the beam. Also, it was shown that by adding variable stiffness layers to the spar, it is possible to either remove the resonance crossings from the operational speed range of the rotor or shift them towards higher harmonics. Furthermore, the number of variable stiffness layers directly impacts the speed at which the resonance happens. Finally, a full-scale blade with variable stiffness spar was considered where the results indicated that this concept has the potential to be used for resonance avoidance of variable speed rotor. Further research is necessary to be performed to investigate how this concept can influence the vibratory loads of the blade.

6. References

[1] I. Goulos, V. Pachidis, R. d'Ippolito, J. Stevens, and C. Smith, "An Integrated Approach for the Multidisciplinary Design of Optimum Rotorcraft Operations," *Journal of Engineering for Gas Turbines and Power,* vol. 134, no. 9, 2012.

[2] R. Chandrasekaran and D. H. Hodges, "Load Reduction During Resonance Crossing of a Variable-Speed Rotor," *Journal of Aircraft,* vol. 60, no. 1, pp. 97-119, 2023.

[3] R. Dibble, V. Ondra, and B. Titurus, "Resonance avoidance for variable speed rotor blades using an applied compressive load," *Aerospace Science and Technology,* vol. 88, pp. 222-232, 2019/05/01/ 2019.

[4] I. Goulos and M. Bonesso, "Variable rotor speed and active blade twist for civil rotorcraft: Optimum scheduling, mission analysis, and environmental impact," *Aerospace Science and Technology,* vol. 88, pp. 444-456, 2019/05/01/ 2019.

[5] G. A. Misté and E. Benini, "Variable-Speed Rotor Helicopters: Performance Comparison Between Continuously Variable and Fixed-Ratio Transmissions," *Journal of Aircraft,* vol. 53, no. 5, pp. 1189-1200, 2016.

[6] R. W. Prouty, *Helicopter Aerodynamics*. Philips Business Information, Inc., 1985.

[7] J. Steiner, F. Gandhi, and Y. Yoshizaki, "An Investigation of Variable Rotor RPM on Performance and Trim," presented at the American Helicopter Societu, 64th Annual Forum, 2008.
[8] M. Mistry and F. Gandhi, "Helicopter Performance Improvement with Variable Rotor Radius and RPM," *Journal of the American Helicopter Society,* vol. 59, no. 4, pp. 17-35, // 2014.
[9] A. E. Karem, "Optimum speed rotor," United States Patent 6, 007, 298, 28 December 1999.
[10] S. Jayatilake, J. Wu, and B. Titurus, "Tendon-inerter-damper helicopter blade augmentation for improved dynamic performance," *Journal of Sound and Vibration,* vol. 547, p. 117509, 2023/03/17/ 2023.
[11] J. Onoda, T. Endo, H. Tamaoki, and N. Watanabe, "Vibration Suppression by Variable-Stiffness Members," *AIAA Journal,* vol. 29, no. 6, pp. 977-983, 1991.
[12] F. Gandhi and S.-G. Kang, "Beams with controllable flexural stiffness," *Smart Materials and Structures,* vol. 16, no. 4, p. 1179, 2007/06/29 2007.
[13] P. C. Chen, D. Sarhaddi, R. Jha, D. D. Liu, K. Griffin, and R. Yurkovich, "Variable Stiffness Spar Approach for Aircraft Maneuver Enhancement Using ASTROS," *Journal of Aircraft,* vol. 37, no. 5, pp. 865-871, 2000.
[14] W. Raither, A. Bergamini, F. Gandhi, and P. Ermanni, "Adaptive bending-twist coupling in laminated composite plates by controllable shear stress transfer," *Composites Part A: Applied Science and Manufacturing,* vol. 43, no. 10, pp. 1709-1716, 2012/10/01/ 2012.
[15] E. A. Allen, L. D. Taylor, and J. P. Swensen, "Smart material composites for discrete stiffness materials," *Smart Materials and Structures,* vol. 28, no. 7, p. 074007, 2019/06/12 2019.
[16] C. A. Rogers, "Active vibration and structural acoustic control of shape memory alloy hybrid composites: Experimental results," *The Journal of the Acoustical Society of America,* vol. 88, no. 6, pp. 2803-2811, 1990.
[17] D. H. Hodges, "Geometrically Exact, Intrinsic Theory for Dynamics of Curved and Twisted Anisotropic Beams," *AIAA Journal,* vol. 41, no. 6, pp. 1131-1137, 2003.
[18] M. R. Amoozgar, H. Shahverdi, and A. S. Nobari, "Aeroelastic Stability of Hingeless Rotor Blades in Hover Using Fully Intrinsic Equations," *AIAA Journal,* vol. 55, no. 7, pp. 2450-2460, 2017.
[19] M. R. Amoozgar, A. D. Shaw, J. Zhang, and M. I. Friswell, "Composite Blade Twist Modification by Using a Moving Mass and Stiffness Tailoring," *AIAA Journal,* vol. 57, no. 10, pp. 4218-4225, 2019.
[20] E. C. Smith and I. Chopra, "Aeroelastic Response, Loads, and Stability of a Composite Rotor in Forward Flight," *AIAA Journal,* vol. 31, no. 7, pp. 1265-1273, 1993.
[21] M. R. Amoozgar, A. D. Shaw, and M. I. Friswell, "The effect of curved tips on the dynamics of composite rotor blades," *Aerospace Science and Technology,* vol. 106, p. 106197, 2020/11/01/ 2020.